

10/2002

GC
7.8
A83
2002

Linear and Nonlinear Rossby Waves in Basins both with and without a Thin Meridional Barrier

by

Juli Atherton

B.S., McGill University (1997)

Submitted to the Joint Program in Physical Oceanography
in partial fulfillment of the requirements for the degree of

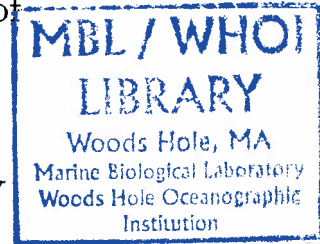
Master of Science

at the

MASSACHUSETTS INSTITUTE OF TECHNOLOGY

and the

WOODS HOLE OCEANOGRAPHIC INSTITUTION



February 2002

© Juli Atherton, MMII. All rights reserved.

The author hereby grants to MIT and WHOI permission to reproduce
and distribute publicly paper and electronic copies of this thesis
document in whole or in part.

Author
Joint Program in Physical Oceanography
Nov 20, 2001

Certified by
Joseph Pedlosky
Senior Scientist
Henry L. and Grace Doherty Oceanographer
Thesis Supervisor

Accepted by
Carl Wunsch
Cecil and Ida Green Professor of Physical Oceanography
Chairman, Joint Committee for Physical Oceanography

10/2002

Linear and Nonlinear Rossby Waves in Basins both with and without a Thin Meridional Barrier

by

Juli Atherton

Submitted to the Joint Program in Physical Oceanography
on Nov 20, 2001, in partial fulfillment of the
requirements for the degree of
Master of Science

Abstract

The linear and nonlinear Rossby wave solutions are examined in homogeneous square basins on the β -plane both with and without a thin meridional barrier. In the presence of the meridional barrier the basin is almost partitioned into two; only two small gaps of equal width, d , to the north and south of the barrier allow communication between the eastern and western sub-basins.

Solutions are forced by a steady periodic wind forcing applied over a meridional strip near the eastern side. Bottom friction is present to allow the solutions to reach equilibrium. The linear solution for the basin containing the barrier is determined analytically and the nonlinear solutions for both basins are found numerically.

In the linear solution with the barrier present, particular attention was paid to the resonant solutions. We examined the effects of varying the symmetry of the forcing about the mid-latitude, the frequency of the periodic forcing and the strength of the bottom friction. For each solution we focus on how the no net circulation condition, which is central to any solution in a barrier basin, is satisfied.

The nonlinear solutions were studied for both basin configurations. In each case the transition from the weakly nonlinear solution to the turbulent solution was examined, as the forcing frequency and forcing strength were varied. Only integer multiples of the forcing frequency are present in the weakly nonlinear solutions. The turbulent solutions were accompanied by the appearance of many other frequencies whose exact origins are unknown, but are probably the result of instabilities.

A hysteresis was found for the turbulent solutions of both the barrier-free and barrier basins.

In the weakly nonlinear solutions of the barrier basin it was predicted and confirmed that there is never a steady net flow from sub-basin to sub-basin. It was also shown that with a symmetric forcing all modes oscillating with an odd multiple of the forcing frequency are symmetric and all modes oscillating with even multiples of the forcing frequency are antisymmetric.

Thesis Supervisor: Joseph Pedlosky
Title: Senior Scientist
Henry L. and Grace Doherty Oceanographer

Acknowledgments

I would like to thank my advisor, Joe Pedlosky, for introducing me to the the problem of studying Rossby modes for various basin configurations and for helping me publish my pregenerals research (presented in chapter 3 of this thesis) in *Il Nuovo Cimento*. I am especially grateful for the way Joe has made himself readily available for discussions and for his promptness in returning my work and providing feedback.

I would also like to thank my committee members Mike Spall, Joe LaCasce, Nelson Hogg, and Glenn Flierl. In particular, I thank Mike Spall for giving me his modified version of MICOM when I began my research.

Special thanks are due to thank my classmate Pablo Zurita who has been a good friend and has helped me immensely in the last few years. Through numerous discussions we have had, I have learnt a great deal me much about computers and numerical computation. This not only helped me to get MICOM running, but has provided me with skills that will be very helpful in the future. I am also grateful to Pablo for allowing me to run MICOM and store my results on his computer.

I am indebted to Brian Arbic who directed the computer Huron my way when he went to Princeton. Huron has been a great benefit to me this last year. I would alsolike to thank Richard Wardle, Francis Poulin, and Samar Khatiwala for interesting discussions regarding this thesis.

Last, but not least, I would like to thank my parents, sister, and Adrian for all their encouragement.

Contents

1	Introduction	15
2	Basin Modes	18
2.1	Barrier-Free Basin	19
2.2	Barrier Basin - Containing Meridional Barrier	20
2.3	Inner Product of Modes	22
2.4	Projection of Solution Onto the Basin Modes	23
3	Linear Barrier Basin Problem	25
3.1	Analytical Solution	25
3.2	Results	31
3.2.1	Symmetric Forcing	32
3.2.2	Antisymmetric Forcing	34
3.2.3	Asymmetric Forcing	34
3.2.4	Bottom Friction	35
3.3	Analysis - Another Look at the QG Equation	37
4	Numerical Model	39
4.1	MICOM Model	39
4.2	QG Dynamics	40
4.3	Numerical Stability and Lateral Friction	43
4.4	Scaling for the Numerical Runs	44

5	Nonlinear Solution for the Barrier-Free Basin	48
5.1	Previous Weakly Nonlinear Results for the Periodically Forced Barrier Basin	48
5.1.1	Bottom Friction and Forcing Larger than the Nonlinearity . .	49
5.1.2	Nonlinearity Larger than the Bottom Friction and Forcing . .	50
5.2	Numerical Results	51
5.3	Description of Results	53
5.4	Analysis of Results	56
6	Nonlinear Solution for the Barrier Basin	62
6.1	Numerical Results	62
6.2	Description of Results	62
6.3	Analysis of Results	66
7	Conclusions	72
A	Tables	76
B	Figures	78
C	Analytical Expression for Variance in the Linear Barrier Basin Problem	117

List of Figures

B-1	Sketch of the square barrier basin with the meridional barrier placed at x_I and the forcing along the dotted line at x_F . There are two gaps of width d to the north and south of the barrier.	79
B-2	Semilog plots of $ \phi_I $ (- -) and (a) full basin variance, (b) eastern sub-basin variance and (c) western sub-basin variance vs forcing frequency $\omega_{F_{n.d}}$ for the case where $x_I = 0.3$, $x_F = 0.7$, $d = 0.05$, $\gamma = 10^{-8}$ and the meridional structure of the forcing is symmetric about $y = 0.5$. . .	80
B-3	Contour plots of the absolute value of the envelope function, $ \phi(x, y) $, for the case where $x_I = 0.3$, $x_F = 0.7$, $d = 0.05$, $\gamma = 10^{-8}$, and the meridional structure of the forcing is symmetric about $y = 0.5$. The forcing frequencies, shown under each plot, correspond to the first 7 peaks in the full basin variance graph in Figure B-2 (a). The value EC shown to the left of each forcing frequency is the circulation on the eastern side of the barrier (see appendix C for calculation of EC) . . .	81
B-4	Semilog plots of (a) full basin variance, (b) eastern sub-basin variance vs forcing frequency $\omega_{F_{n.d}}$. Plots (c) and (d) are contours of the absolute value of the envelope function, $ \phi(x, y) $, at frequencies corresponding to the first two peaks of the full variance. $x_I = 0.3$, $x_F = 0.7$, $d = 0.05$, $\gamma = 10^{-8}$ and antisymmetric meridional structure of the forcing about $y = 0.5$	82

B-5	Semilog plots of $ \phi_I $ (- - -) and (a) full basin variance, (b) eastern sub-basin variance and (c) western sub-basin variance vs forcing frequency $\omega_{F_{n,d}}$ for $x_I = 0.3$, $x_F = 0.7$, $d = 0.05$, $\gamma = 10^{-8}$, and the asymmetric meridional structure of the forcing.	83
B-6	Contour plots for $x_I = 0.3$, $x_F = 0.7$, $d = 0.05$, $\gamma = 10^{-8}$, and the asymmetric meridional structure of the forcing. The forcing frequencies, under each plot, correspond to the first nine peaks in the full basin variance graph in Figure 5 (a). The value EC shown next to the forcing frequency is the circulation on the east side of the barrier (see appendix C for calculation of EC).	84
B-7	Semilog plots of $ \phi_I $ (- - -) and full basin variance vs forcing frequency $\omega_{F_{n,d}}$ for $x_I = 0.3$, $x_F = 0.7$, $d = 0.05$, and asymmetric meridional structure of the forcing, and varying friction (a) $\gamma = 0.0001$, (b) $\gamma = 0.001$, (c) $\gamma = 0.0025$, (d) $\gamma = 0.005$, (e) $\gamma = 0.01$, (f) $\gamma = 0.0167$	85
B-8	The (a) full basin, (b) eastern sub-basin and (c) western sub-basin variance response vs the bottom friction parameter γ for $\omega_{F_{n,d}} = 0.08$ for the barrier basin analytical solution.	86
B-9	Contours of the envelope (i.e. absolute value $ \phi(x, y) $) for $\omega_{F_{n,d}} = 0.08$ and certain values of the bottom friction parameter γ in the linear barrier basin solution. (a) $\gamma = 0.005$, (b) $\gamma = 0.01$, (c) $\gamma = 0.015$, (d) $\gamma = 0.02$	87
B-10	Amplitude response curve calculated using the method presented in [3] The parameters $k = 0$, $m = 2$, $n = 1$, $f = 1$, and, $\delta = 0.126$ correspond to our first numerical run where $\left(\frac{\delta L}{L}\right)_{WN}^2 = 0.002$	88
B-11	Mean integrated kinetic energy vs forcing frequency, $\omega_{F_{n,d}}$, for the series of numerical runs with increasing nonlinearity. Notice how the peaks lean towards higher frequencies and then ultimately disintegrate. Also, note the transition in the solution occurring at the nondimensional frequencies $\omega_{F_{n,d}}$, 0.0775, 0.08, 0.0875, and 0.085 for the wind forcing strengths $\left(\frac{\delta L}{L}\right)_{WN}^2 = 0.004, 0.006, 0.008, \text{ and } 0.01$, respectively.	89

- B-12 Envelopes calculated over one forcing period demonstrating that the weakly nonlinear solution is dominated by the (2, 1) mode just before the transition which occurs when the forcing frequency is decreased. (a) $\left(\frac{\delta_I}{L}\right)_{WN}^2 = 0.004$ and $\omega_{Fn.d.} = 0.0775$, (b) $\left(\frac{\delta_I}{L}\right)_{WN}^2 = 0.006$ and $\omega_{Fn.d.} = 0.0825$, (c) $\left(\frac{\delta_I}{L}\right)_{WN}^2 = 0.008$ and $\omega_{Fn.d.} = 0.085$, and (d) $\left(\frac{\delta_I}{L}\right)_{WN}^2 = 0.01$ and $\omega_{Fn.d.} = 0.0875$ 90
- B-13 Envelope plots taken over one forcing period showing the solution just after the transition to the very nonlinear solution when the forcing frequency is decreased. (a) $\left(\frac{\delta_I}{L}\right)_{WN}^2 = 0.004$ and $\omega_{Fn.d.} = 0.0775$, (b) $\left(\frac{\delta_I}{L}\right)_{WN}^2 = 0.006$ and $\omega_{Fn.d.} = 0.0825$, (c) $\left(\frac{\delta_I}{L}\right)_{WN}^2 = 0.008$ and $\omega_{Fn.d.} = 0.085$, and (d) $\left(\frac{\delta_I}{L}\right)_{WN}^2 = 0.01$ and $\omega_{Fn.d.} = 0.0875$ 91
- B-14 Contours of the stream function, Ψ , at 2 day intervals for the solution $\left(\frac{\delta_I}{L}\right)_{WN}^2 = 0.004$ and $\omega_{Fn.d.} = 0.0725$. The contours span 24 days of the 25.08 day forcing period. Solid lines correspond to positive stream lines and dotted lines correspond to negative streamlines. The contours document the westward propagation of the solution during one forcing period. Note NL in the figure denotes $\left(\frac{\delta_I}{L}\right)_{WN}^2$ 92
- B-15 Contours of the stream function, Ψ , at 2 day intervals for the solution $\left(\frac{\delta_I}{L}\right)_{WN}^2 = 0.01$ and $\omega_{Fn.d.} = 0.0725$. The contours span 24 days of the 25.08 day forcing period. Solid lines correspond to positive stream lines and dotted lines correspond to negative streamlines. The contours document the westward propagation of the solution during one forcing period. Note NL in the figure denotes $\left(\frac{\delta_I}{L}\right)_{WN}^2$ 93
- B-16 The maximum zonal and meridional velocities plotted vs the nondimensional forcing frequencies, $\omega_{Fn.d.}$, for each set of nonlinear runs. Note NL in the figure denotes $\left(\frac{\delta_I}{L}\right)_{WN}^2$ 94
- B-17 Fourier transform of the zonal velocity at the point (800km, 800km) for the nonlinear solutions with a forcing frequency of $\omega_{Fn.d.} = 0.0725$. Note NL in the figure denotes $\left(\frac{\delta_I}{L}\right)_{WN}^2$ 95

- B-18 Contour plots of the absolute values of the spatial coefficients of the terms in a Fourier time series which oscillate at frequencies that are integral multiples of the forcing frequencies. Note NL in the figure denotes $\left(\frac{\delta_I}{L}\right)_{WN}^2$ 96
- B-19 Fourier transform of the zonal velocity for different points in the basin at mid-latitude over 1200 days (a) east side, (b) middle, (c) west side. $\left(\frac{\delta_I}{L}\right)_{WN}^2 = 0.004$ and $\omega_{Fn.d.} = 0.0725$, note higher frequencies appearing as we proceed west. 97
- B-20 Finite difference calculation of the model output for the terms in the QG equation excluding the forcing term. $\left(\frac{\delta_I}{L}\right)_{WN}^2 = 0.008$ and $\omega_{Fn.d.} = 0.085$. This is just before the solution transitions to the turbulent regime at $\omega_{Fn.d.} = 0.0825$. Note NL in the figure denotes $\left(\frac{\delta_I}{L}\right)_{WN}^2$ 98
- B-21 Finite difference calculation of the model output for the terms in the QG equation excluding the forcing term. The solution has a wind forcing strength $\left(\frac{\delta_I}{L}\right)_{WN}^2 = 0.008$ and a forcing frequency $\omega_{Fn.d.} = 0.0825$. This is just after the transition to the turbulent regime. Note NL in the figure denotes $\left(\frac{\delta_I}{L}\right)_{WN}^2$ 99
- B-22 Mean integrated kinetic energy vs nondimensional forcing frequency, $\omega_{Fn.d.}$. The results plotted by squares indicates that the solution was initialized with zero initial conditions. The results plotted with the asterisk indicate that each run was initialized with the results of the previous run forced at the lower forcing frequency. A hysteresis is observed for the forcing frequencies $\omega_{Fn.d.} = 0.085$ for zero initial conditions and $\omega_{Fn.d.} = 0.09$ for initial conditions of lower frequency run. 100
- B-23 (a) is the RMS of the stream function just before the transition and (b) is the RMS of the stream function just after the transition when the solution is in its weakly nonlinear state. These runs have been initialized with solutions forced at a lower frequency. Note NL in the figure denotes $\left(\frac{\delta_I}{L}\right)_{WN}^2$ 101

B-24	Mean integrated kinetic energy over the area of the barrier basin vs forcing frequency for runs with forcing strengths of $\left(\frac{\delta L}{L}\right)_{WN}^2 = 0.004$ and 0.01 respectively. All runs were done with zero initial conditions.	102
B-25	The contours of the envelope function for all the solutions forced with a strength $\left(\frac{\delta L}{L}\right)_{WN}^2 = 0.004$ and zero initial conditions.	103
B-26	The contours of the envelope function for all the solutions forced with a strength $\left(\frac{\delta L}{L}\right)_{WN}^2 = 0.01$ and zero initial conditions. Note the slight change in the nonlinearity of the solution in the eastern basin between the frequencies $\omega_{F_{n.d.}} = 0.075$ and $\omega_{F_{n.d.}} = 0.0775$. The solution forced with a frequency of $\omega_{F_{n.d.}} = 0.0775$ looks more linear than the the solution forced at $\omega_{F_{n.d.}} = 0.075$.	104
B-27	Contours of the stream function, Ψ , at 2 days intervals for the solution $\left(\frac{\delta L}{L}\right)_{WN}^2 = 0.004$ and $\omega_{F_{n.d.}} = 0.0725$ in the barrier basin. The contours span 24 days of the 25.08 day forcing period. Solid lines correspond to positive stream lines and dotted lines correspond to negative stream lines. The contours document the westward propagation of the solution during one forcing period.	105
B-28	Contours of the stream function, Ψ , at 2 days intervals for the solution $\left(\frac{\delta L}{L}\right)_{WN}^2 = 0.01$ and $\omega_{F_{n.d.}} = 0.0725$ in the barrier basin. The contours span 24 days of the 25.08 day forcing period. Solid lines correspond to positive stream lines and dotted lines correspond to negative stream lines. The contours document the westward propagation of the solution during one forcing period.	106
B-29	Contour plots of Ψ at two day intervals for the solution $\left(\frac{\delta L}{L}\right)_{WN}^2 = 0.01$ and $\omega_{F_{n.d.}} = 0.0725$. The barrier is placed at 1420km to the east and the wind forcing is applied along a meridional strip from 200km to 400km.	107

B-30 Fourier transform of the zonal velocity at points along the mid-latitude.
(a), (c), and (e) are the solutions for $\left(\frac{\delta L}{L}\right)_{WN}^2 = 0.01$ and $\omega_{F_{n.d.}} = 0.0725$, while (b), (d), and (f) are the solutions for $\left(\frac{\delta L}{L}\right)_{WN}^2 = 0.004$ and $\omega_{F_{n.d.}} = 0.0725$. (a) and (b) are the Fourier transforms of velocities in the west of the basin, (c) and (d) are Fourier transforms in the middle, and (e) and (f) are Fourier transforms in the west of the basin. 108

B-31 Fourier transforms of the zonal velocity for solutions forced at 0.0725 and increasing wind strength. Figures (a), (b) and (c) indicate that as the forcing strength increases the first non-integer multiple of the forcing frequency to appear is at about 0.1 which is close to $\frac{3}{2}$ times $\omega_{F_{n.d.}}$ or the natural frequency of the first resonant mode in the barrier basin. 109

B-32 Envelope plot for the spatial coefficients associated with the peaks labeled 1,2,3,4,5, and 6 in Figure B-30 (a) corresponding to the solution $\left(\frac{\delta L}{L}\right)_{WN}^2 = 0.004$ and $\omega_{F_{n.d.}} = 0.0725$ 110

B-33 (a) plots the Fourier transform of the zonal velocity at a point. The peak labels, 0, 2, 4, and 6, correspond to the labels in Figure B-30 (b). (b), (c), (d), and (e) above are the absolute values of the spatial coefficients corresponding to peaks 0, 2, 4, and 6 labeled in (a). 111

B-34 (a) plots the Fourier transform of the zonal velocity at a point. The peak are labeled correspond their relation to the forcing frequency, $\omega_{F_{n.d.}}$. (b), (c), and (d) above are the absolute values of the spatial coefficients corresponding to peaks labeled in (a). 112

B-35 Mean integrated kinetic energy for the solutions forced with a strength of $\left(\frac{\delta L}{L}\right)_{WN}^2 = 0.01$ in the barrier basin. The six pointed star represents solutions initialized with zero initial conditions and the circle represents the solution forced at $\omega_{F_{n.d.}} = 0.0775$ initialized with the solution of $\omega_{F_{n.d.}} = 0.075$ 113

- B-36 The asterisks, *, represent the mean integrated kinetic energy of the solution initialized with zero initial conditions for a wind forcing of $\left(\frac{\delta L}{L}\right)_{WN}^2 = 0.01$ and bottom friction $\frac{\delta s}{L} = 0.001$. The circles, (o), represent the mean integrated kinetic energy of the solution forced with a nondimensional frequency of $\omega_{F_{n.d.}} = 0.0775$ and initialized with the solution which was forced at $\omega_{F_{n.d.}} = 0.075$ 114
- B-37 The dotted line plots the mean integrated kinetic energy vs the time in model days of the run forced with $\omega_{F_{n.d.}} = 0.0775$, $\left(\frac{\delta L}{L}\right)_{WN}^2 = 0.01$ and $\frac{\delta s}{L} = 0.001$ and initialized with zero initial conditions. The solid line represents the corresponding run initialized with the solution from the lower forcing frequency $\omega_{F_{n.d.}} = 0.075$ 115
- B-38 Contour plots of envelope for solutions forced at $\left(\frac{\delta L}{L}\right)_{WN}^2 = 0.01$, $\frac{\delta s}{L} = 0.001$, and $\omega_{F_{n.d.}} = 0.0775$. (a) initialized with zero initial conditions and (b) initialized with the solution forced at $\omega_{F_{n.d.}} = 0.075$ 116

List of Tables

A.1	Comparison of the nine resonant solutions in Figures B-5 and B-6 to the normal modes for a barrier-free basin to which they resemble. The resemblance is observed both in the structure of the solution and in the frequencies. For the case where the dominant response is in a sub-basin we consider a basin the same size. The quotation marks indicate that a sub-basin solution is symmetric and hence is part of the subset of full basin modes and not a part of the set of antisymmetric sub-basin modes.	77
-----	---	----

